WITHDRAWN:
Heat and mass transport characteristics of microchannel steam reforming reactor systems for hydrogen production

Junjie Chen

cjjmmm@163.com

Henan Polytechnic University https://orcid.org/0000-0001-8348-4896

Lingyu Meng

Henan Polytechnic University

Research Article

Keywords: Microchannel reactors, Steam reforming, Hydrogen production, Endothermic reactions, Transport characteristics, Computational fluid dynamics

Posted Date: May 19th, 2022

DOI: https://doi.org/10.21203/rs.3.rs-1671054/v1

EDITORIAL NOTE:

The full text of this preprint has been withdrawn by the authors while they make corrections to the work. Therefore, the authors do not wish this work to be cited as a reference. Questions should be directed to the corresponding author.

Abstract

Chemical reactions that produce heat and those that take up heat form two very important classes of reactions. Although exothermic and endothermic reactions are easy to implement, a compact and simple reactor design is challenging due to the limitations of heat and mass transport. The present study relates to a catalytic process of methanol steam reforming for the production of hydrogen in a microchannel steam reforming reactor system. Processes of conducting endothermic steam reforming reactions in integrated combustion reactors were described. The effect of washcoat thickness on reaction and transport processes were investigated in terms of efficiency and performance. The importance of effectiveness factor was highlighted. Engineering maps that delineated temperature, species mole fractions, sensible enthalpy, and total enthalpy were constructed. Design recommendations were made to improve the overall heat and mass transport characteristics. The results indicated that the reactor system is capable of high heat and mass transfer coefficients between a bulk reaction fluid and the catalytic heat exchange surface. The thickness of catalyst washcoats are fundamentally important for improving the overall transport characteristics. A desired level of reactor performance can be maintained through the use of optimum key parameters pertaining to the chemically reacting flow system. However, to ensure the effectiveness of the endothermic steam reformation process, the catalyst washcoats must be sufficiently thick. The thickness of catalyst washcoats can be tailored to avoid the limitations imposed by heat transfer and chemical kinetics.

1. Introduction

Packed beds are most often preferred for adiabatic catalytic reactors at least partly because the particles in the bed are relatively inexpensive to produce and can be made to conform to vessels with large cross-sectional area to lower substantial pressure drops, where intentional heat transfer is not as highly valued as these other characteristics [1, 2]. Structured packings in the form of honeycombs generally have the lowest ratio of pressure drop to mass transfer for situations where the cross-sectional area of the reactor is confined and low pressure-drop is required [3, 4], such as in the after treatment of exhaust from an engine [5, 6]. Honeycomb reactors are preferred in reactors of confined cross-section where heat transfer to increase the equilibrium constant of the given intended reaction is not substantial or intentional [7, 8]. Honeycombs generally are in the form of a catalytic coating on a substrate composed of ceramic or metal walls defining straight channels which are parallel to each other and to the axis of the reactor [7, 8]. Relatively high mass transfer is provided by using high cell density channels, namely, low hydraulic diameter channels [9, 10]. Structured packings in the form of honeycombs provide poor heat transfer because they may increase the number of boundary layers between a fluid and a reactor wall by a factor of one hundred or more [11, 12], where boundary layers are known to impede heat transfer.

In some processes, it is desirable to conduct endothermic or exothermic reactions substantially isothermally [13, 14] or to conduct endothermic reactions at progressively higher temperatures as in steam methane reforming [15] or exothermic reactions at progressively lower temperatures as in methanol synthesis from mixtures of hydrogen and carbon monoxide [16] or in ammonia synthesis from mixtures of hydrogen and nitrogen [17] or as in hydrogenation, methanation, or water gas shift reactions [18]. In such

processes, defined herein as non-adiabatic, some amount of intentional heat transfer is needed. Packed beds have been preferred historically for non-adiabatic catalytic reactors [19, 20] at least partly because packed beds are generally less expensive than structured packings. Packed beds of extruded pellets can also have thick walls and higher concentrations of kinetically active ingredients to contain higher catalyst surface area than structured packings [21, 22], which is advantageous for processes limited or controlled by the kinetic rates of the reaction sites as opposed to the rate of heat transfer or mass transfer to or from the reaction sites. Packed beds also induce turbulence and fluid flow against reactor walls to break down boundary layers that would otherwise impede heat transfer [23, 24], which is desirable in processes controlled or limited by heat transfer.

More recently, it has been found that structured packings can be engineered to provide a higher ratio of heat transfer to pressure drop than packed beds in similar catalytic processes [25, 26]. However, these and other structured packings and packed beds have undesirably high ratios of pressure drop to mass transfer between the bulk fluid and the reaction sites [27, 28], herein referred to as mass transfer. Some structured packings with channels parallel to the reactor axis have been proposed for processes controlled by heat transfer [29, 30]. Structured packings incorporate straight channels parallel to the reactor axis in a non-adiabatic reactor, but each of these structured packings entails blockage or masking of a significant part of the reactor cross-section to increase the fluid velocity and thereby increase the heat transfer into the reactor for the steam methane reforming process [31, 32]. In many cases, structured packings achieve improved heat transfer compared to packed beds by using measures to increase pressure drop to levels almost as high or as high as in packed beds for applications controlled by heat transfer [33, 34]. Significant effort has been expended to effectively improve heat transfer and reduce pressure drop by using microchannel process technology for the purposes of reactor design from both physical and chemical perspectives [35, 36]. For example, the use of a flow-by catalyst configuration for one or both the exothermic and endothermic microchannels can create an advantageous capacity-pressure drop relationship [37, 38]. While steam reforming in microchannel reactors is feasible, the interplay of transport and kinetics in the performance characteristics of these small-scale high-throughput systems is poorly understood. Despite extensive study of the process of steam reforming in microchannel reactor systems [39, 40], the effects of heat and mass transfer on efficiency and performance have not been well studied. Further study is needed to the heat and mass transport characteristics of microchannel steam reforming reactor systems.

The present study is directed to a microchannel steam reforming reactor system, which can simultaneously carry out endothermic and exothermic reactions in separate microchannels. Specifically, the present study relates to a catalytic process of steam-methanol reforming for the production of hydrogen in a microchannel steam reforming reactor system, and the walls separating adjacent endothermic and exothermic reaction channels are thermally conductive. In the present study, computational fluid dynamics simulations were performed with respect to various factors pertaining to the reactor system. Steady-state analyses were carried out to investigate the effects of various key parameters on processes such as chemical reactions or heat and mass transfer in the reactor system. The importance of effectiveness factor was highlighted. Engineering maps that delineated temperature, species mole fractions, sensible enthalpy, and total enthalpy were constructed. Design recommendations were made to improve the overall heat and

mass transport characteristics. The objective is to investigate the heat and mass transport characteristics of microchannel steam reforming reactor systems for hydrogen production. Particular emphasis is placed on the dependence of reaction and transport processes on various factors pertaining to the reactor system.

2. Numerical Methods

2.1. Description of the reactor system

The study relates to a catalytic process for the production of hydrogen by steam reforming of methanol, in which methanol and steam are reacted in a microchannel steam reforming reactor system under relatively high pressure. Steam reforming of methanol have attracted much attention for applications in fuel cells [41, 42]. The microchannel steam reforming reactor system is schematically depicted in Fig. 1 for purposes of illustration. The autothermal reactor is configured for simultaneous combustion and steam reformation of methanol. Exothermic and endothermic reactions take place simultaneously whereby the heat required for the latter is supplied by the former. Heat transfer occurs via conduction through the walls of the reactor. There are multiple possibilities for the arrangement of the combustion channels and the reforming channels for heating, such as co-current, countercurrent, or cross-flow modes. In the present study, the two separate sets of flow channels are arranged in a co-current flow configuration. The reactor system is operated using excess air and water steam. Methanol and air are mixed homogeneously and the mixture is fed directly into the combustion channels in a specific ratio. Preferably, excess water steam is provided to the reactor to increase efficiency and to maintain operability, for example, to prevent carbon formation. Such a reactor system is typically adiabatic in nature, meaning no heat is added in addition to the exothermic reaction heat release. The reactor system offers relatively simple designs and operation.

The reactor system is in the form of a catalytic coating on a substrate composed of ceramic or metal walls defining straight reforming or combustion channels which are parallel to each other and to the axis of the reactor. Relatively high mass transfer is provided by using high cell density channels, namely low hydraulic diameter channels. The design increases the number of boundary layers between a fluid and a reactor wall by a factor of one hundred or more, and boundary layers are known to impede heat transfer. However, relatively high heat transfer is provided. All channels are of the same cross-section and length. Additionally, there are equal numbers of combustion and reforming channels, which are arranged in an alternating pattern. The wall of each channel is composed of a substrate coated with a catalyst. The substrate is preferably metal, and most preferably stainless-steel sheet, for example, Fecralloy™ used in the present study. In the present study, the cross-sectional configuration of the channels is square. The channels are 0.7 mm in height and in width and 50.0 mm in length. Channel height refers to the inside height of a channel. To ensure the mechanical strength at elevated pressures, the thickness of the uncoated walls and the catalyst washcoats is 0.7 and 0.1 mm, respectively. The combustion catalyst consists essentially of oxides of copper, zinc and aluminum. The combustion catalyst allows for initial start-up and the heat-up of the reactor system. The reforming catalyst consists essentially of copper and oxides of zinc and aluminum. The exothermic and endothermic processes are conducted at a pressure of 0.8 MPa, with a methanol-air equivalence ratio of 0.8 and a steam-to-methanol molar ratio of 1.4. The inlet temperature of the mixtures

is 373 K. The temperature of the reactor can be regulated by the balance of the flow rates so that the catalyst is not overheated by the exothermic process and thus damaged.

2.2. Mathematical model of the reactor system

To facilitate computational modeling of transport phenomena and chemical kinetics in the flowing system of complex chemical reactions involving gas-phase and surface species, steady-state analyses are performed and computational fluid dynamics is used.

A surface reaction mechanism is assumed to involve K_s chemical species with I surface reactions. This reaction mechanism can be represented in the following general form

$$\sum_{s=1}^{K_s} \nu'_{si} \chi_s \Leftrightarrow \sum_{s=1}^{K_s} \nu''_{si} \chi_s, \ (i=1, \ldots, I)$$

1

,

wherein χ_s is the chemical symbol for surface species s, ν_{si} is the stoichiometric coefficient for surface reaction i with surface species s, which is positive for both reactants and products, ν'_{si} is the stoichiometric coefficient described for reactants, and ν''_{si} is the stoichiometric coefficient described for products.

The production rate $\dot{s}_s$ for each of surface species can be written as a sum over the rate-of-progress variables for all reactions involving surface species s:

$$\dot{s}_s = \sum_{i=1}^{I} v_{si} q_i, \ (s=1, \ldots, K_s)$$

2

,

$$v_{si} = v''_{si} - v'_{si}$$

3

,

where the chemical production rate of surface species s is denoted by $\dot{s}_s$, and the rate-of-progress variable for surface reaction i is denoted by q_i.

The rate-of-progress variable for surface reaction i is given by the difference of the forward rates and the reverse rates as follows:

$$q_i = k_{fi} \prod_{s=1}^{K_s} [\chi_s]^{v'_{si}} - k_{ri} \prod_{s=1}^{K_s} [\chi_s]^{v''_{si}}$$

4

,

wherein $[\chi_s]$ is the molar concentration of surface species *s*, *k* is the rate constant, k_{fi} is the forward rate constant of surface reaction *i*, and k_{ri} is the reverse rate constant of surface reaction *i*.

The forward rate constant of surface reaction *i* as a function of thermodynamic temperature is given by the modified Arrhenius expression as follows:

$$k_{fi}=A_i T^{\beta_i} e^{\frac{-E_i}{RT}}$$

5

,

in which A_i is the pre-exponential factor of surface reaction *i*, β_i is the dimensionless temperature exponent of surface reaction *i*, and E_i is the activation energy of surface reaction *i*.

The reverse rate constant of surface reaction *i* involved in reaching equilibrium is related to the forward rate constant through the equilibrium constant, which has the following form:

$$k_{ri}=\frac{k_{fi}}{K_{ci}}$$

6

,

in which K_{ci} is the equilibrium constant of surface reaction *i*. The equilibrium constant is given in concentration units.

The effectiveness factor is given by the Thiele modulus *Φ* as

$$\eta_g=\frac{\dot{s}'_g}{\dot{s}_g}=\frac{\tanh(\Phi)}{\Phi}$$

7

,

wherein $\dot{s}'$ refers to the effective production rate. Species *i* is denoted by the subscript *i*. The Thiele modulus for the chemical reactions can be expressed using the following equation:

$$\Phi=\delta\sqrt{\frac{\gamma\dot{s}_g}{c_g D_g}}$$

8

,

wherein δ is the thickness of a catalyst substrate, γ is the catalyst specific surface area, c is the surface concentration, and D is the effective diffusivity.

Catalyst specific surface area is a property of substrates, defined as the catalyst specific surface area divided by the volume of the substrate that holds or supports a catalyst in a reactor

$$\gamma = \frac{A_c}{V_c}$$

9

,

in which V_c is the volume of a catalyst substrate.

The porous media model is applied to the computational domains of the catalytically active layers. The porous media involve surface reactions. The dependence of the effective diffusivity on porosity and tortuosity factor can be expressed using the following equation:

$$\frac{1}{D_g} = \frac{1}{\varepsilon_p}\tau_p \left(\frac{1}{D_g^m} + \frac{1}{D_g^K} \right)$$

10

.

in which ε_p is the porosity, τ_p is the tortuosity factor, and D^K is the Knudsen diffusivity. The porosity is isotropic. The porosity does not vary with space and therefore the porous media are homogeneous.

2.3. Chemical kinetic models

The equation for the catalytic combustion reaction can be denoted as follows:

$$\mathrm{CH_3OH} + 1.5\mathrm{O_2} \;\Leftrightarrow\; 2\mathrm{H_2O} + \mathrm{CO_2}\,,\, \Delta_r H_m\,(298.15\ \mathrm{K}) = -726.60\ \mathrm{kJ \cdot mol^{-1}}, \quad (11)$$

wherein the standard molar enthalpy of reaction is denoted by $\Delta_r H_m$.

Methanol can be catalytically reformed according to the following equation:

$$\mathrm{CH_3OH} + \mathrm{H_2O} \;\Leftrightarrow\; 3\mathrm{H_2} + \mathrm{CO_2}\,,\, \Delta_r H_m\,(298.15\ \mathrm{K}) = 49.37\ \mathrm{kJ \cdot mol^{-1}}. \quad (12)$$

Methanol can be catalytically decomposed to hydrogen and carbon monoxide in accordance with the following equation:

$$\mathrm{CH_3OH} \;\Leftrightarrow\; 2\mathrm{H_2} + \mathrm{CO}\,,\, \Delta_r H_m\,(298.15\ \mathrm{K}) = 90.47\ \mathrm{kJ \cdot mol^{-1}}. \quad (13)$$

In order to convert carbon monoxide into carbon dioxide, a further water-gas shift reaction is needed, which can be denoted as follows:

$$\mathrm{CO} + \mathrm{H_2O} \;\Leftrightarrow\; \mathrm{H_2} + \mathrm{CO_2}\,,\Delta_r H_m\left(298.15\ \mathrm{K}\right) = -41.10\ \mathrm{kJ}\cdot\mathrm{mol}^{-1}. \quad (14)$$

Therefore, the reformate provided from the reactor is enriched in hydrogen.

The exothermic process is modeled by the chemical kinetic model developed by Reitz *et al*. [43]. Additionally, the endothermic process is modeled in such a way as to take into account methanol steam reforming and decomposition and the water-gas shift reaction using the chemical kinetic model proposed by Peppley *et al*. [44]. The rate of the methanol-steam reforming reaction r_R is expressed by partial pressures

$$r_R = \left[k_R K^*_{\mathrm{CH_3O}^{(1)}}\left(p_{\mathrm{CH_3OH}} p_{\mathrm{H_2}}^{-0.5}\right)\left(1 - k_R^{-1} p_{\mathrm{H_2}}^3 p_{\mathrm{CO_2}} p_{\mathrm{CH_3OH}}^{-1} p_{\mathrm{H_2O}}^{-1}\right) C_{S_1}^T C_{S_{1a}}^T\right]$$
$$\cdot\left[\left(1 + K^*_{\mathrm{CH_3O}^{(1)}}\left(p_{\mathrm{CH_3OH}} p_{\mathrm{H_2}}^{-0.5}\right) + K^*_{\mathrm{HCOO}^{(1)}} p_{\mathrm{CO_2}} p_{\mathrm{H_2}}^{0.5} + K^*_{\mathrm{OH}^{(1)}}\left(p_{\mathrm{H_2O}} p_{\mathrm{H_2}}^{-0.5}\right)\right)\left(1 + K_{\mathrm{H}^{(1a)}}^{0.5} p_{\mathrm{H_2}}^{0.5}\right)\right]^{-1}$$

15

,

wherein the total surface concentration of site *i* is denoted by $C_{S_i}^T$, the composite parameter and the species adsorbed on active site *i* are represented by the superscript $*$ and (*i*), respectively, and the species index is represented by the subscripts 1 and 1*a*.

The rate of the water-gas shift reaction r_W is given by

$$r_W = \left[k_W^* K^*_{\mathrm{OH}^{(1)}}\left(p_{\mathrm{CO}} p_{\mathrm{H_2O}} p_{\mathrm{H_2}}^{-0.5}\right)\left(1 - k_W^{-1} p_{\mathrm{H_2}} p_{\mathrm{CO_2}} p_{\mathrm{CO}}^{-1} p_{\mathrm{H_2O}}^{-1}\right) C_{S_1}^{T^2}\right]$$
$$\cdot\left[\left(1 + K^*_{\mathrm{CH_3O}^{(1)}}\left(p_{\mathrm{CH_3OH}} p_{\mathrm{H_2}}^{-0.5}\right) + K^*_{\mathrm{HCOO}^{(1)}} p_{\mathrm{CO_2}} p_{\mathrm{H_2}}^{0.5} + K^*_{\mathrm{OH}^{(1)}}\left(p_{\mathrm{H_2O}} p_{\mathrm{H_2}}^{-0.5}\right)\right)\right]^{-2}$$

16

.

The rate of the methanol decomposition reaction r_D is given by

$$r_D = \left[k_D K^*_{\mathrm{CH_3O}^{(2)}}\left(p_{\mathrm{CH_3OH}} p_{\mathrm{H_2}}^{-0.5}\right)\left(1 - k_D^{-1} p_{\mathrm{H_2}}^2 p_{\mathrm{CO}} p_{\mathrm{CH_3OH}}^{-1}\right) C_{S_2}^T C_{S_{2a}}^T\right]$$
$$\cdot\left[\left(1 + K^*_{\mathrm{CH_3O}^{(2)}}\left(p_{\mathrm{CH_3OH}} p_{\mathrm{H_2}}^{-0.5}\right) + K^*_{\mathrm{OH}^{(2)}}\left(p_{\mathrm{H_2O}} p_{\mathrm{H_2}}^{-0.5}\right)\right)\left(1 + K_{\mathrm{H}^{(2a)}}^{0.5} p_{\mathrm{H_2}}^{0.5}\right)\right]^{-1}$$

17

,

wherein the species index is represented by the subscripts 2 and 2*a*.

2.4. Numerical algorithms

To obtain the solution of the problem, numerical simulations are performed using computational fluid dynamics. The problem is solved using structured meshes. The typical mesh is depicted in Fig. 2 for the reactor system. The mesh is refined in the computational domains of the catalytically active layers. A mesh independence study is carried out. The solution is independent of the mesh resolution. The governing equations are solved numerically for the conservation of mass and momentum and for energy and species. The governing equations are discretized in space, and the second-order upwind discretization scheme is used. The pressure-based segregated algorithm is used with SIMPLE-type pressure-velocity coupling. The under-relaxation factors are reduced for all variables.

2.5. Validation of the model

A general and flexible framework is provided above for describing the model involving complex transport phenomena and chemical kinetics. Predetermined boundary conditions may be necessary in order to exactly matches the specifications or requirements. To verify the accuracy of the model, the predictions are compared with the data obtained from experimental measurements [45, 46]. The channels are rectangular in cross section. The channels have a width of 0.5 mm, a height of 0.6 mm, and a length of 33.0 mm [45, 46]. Hydrogen is produced by steam reformation at a specific temperature. The reactor operates with a steam-to-carbon molar ratio of 1.1, and the temperature of the endothermic process stream ranges from 473 to 533 K. The rate of hydrogen production predicted by the model are plotted in Fig. 3 against temperature for the reactor system. The predictions are in satisfactory agreement with the data obtained from experimental measurements.

3. Results And Discussion

3.1. Overall characteristics

The contour plots of temperature, species mole fractions, sensible enthalpy, and total enthalpy are presented in Fig. 4 for the reactor system. The thermal conductivity of the wall material is 18 W/(m·K) at room temperature. The energy which is released during catalytic combustion is necessary for the endothermic steam reformation taking place simultaneously, as illustrated in Fig. 4. The energy released upon catalytic oxidation is just sufficient for the conversion of methanol and water steam into a hydrogen-rich gas to occur simultaneously. Methanol is used for the steam reformation, which lowers the temperature of the reactor and minimizes the production of nitrogen oxides during combustion. The temperature of the reactor system is much lower than the deterioration temperature of each catalyst material. Additionally, high reforming efficiencies and the desired thermal efficiencies can be achieved. Methanol breakthrough is negligible, as illustrated in Fig. 4. However, the reactor system must be operated using a stoichiometric or lean fuel-air mixture, making the combustion unstable, making temperature regulation more difficult, and easily allowing undesired nitrogen oxides to arise. Stable temperature regulation is made possible and the endothermic and exothermic reactions are conducted substantially isothermally, as illustrated in Fig. 4. This is because the walls are highly conductive. The carbon monoxide produced in the endothermic process, which would be harmful for a fuel cell system connected

downstream from the reactor system, can be largely converted into carbon dioxide and additional hydrogen through a shift reaction with water, as illustrated in Fig. 4. The hydrogen-rich and sufficiently carbon monoxide-poor product gas is available at the outlet of the reactor as a reformation gas. Therefore, the benefits of using methanol as a fuel for the reforming process are surprisingly great.

3.2. Sensible enthalpy

The effect of washcoat thickness on the sensible enthalpy of the endothermic steam reformation process is illustrated in Fig. 5 for the reactor system. The washcoat thickness varies from 0.04 to 0.20 mm. The velocity of the endothermic process stream and the exothermic process stream is 2.0 and 0.6 m/s, respectively, at the reactor inlets. The catalytic combustion reaction is started especially rapidly to achieve the desired temperature within the reactor system. The heat produced by catalytic combustion of methanol in the first set of flow channels is transferred to the second set of flow channels where a catalytic reforming reaction takes place. The reactor system can be heated very rapidly from the inside, as illustrated in Fig. 5. The design allows the autothermal reactor to be brought to operating temperature in an especially simple way. For the chemically reacting flow system, the sensible enthalpy increases with increasing the thickness of the catalyst washcoats. The reactor system may include a structured packing disposed within the flow channels, wherein the structured packing comprises one or more second walls defining one or more channels for fluid flow through the structured packing. The chemically reacting flow system described herein is a non-adiabatic catalytic reactor, which refers to a catalytic reactor for an endothermic reaction that is externally heated to cause fluid exiting the reactor to have a temperature substantially the same as or hotter than the temperature of the fluid entering the reactor. Therefore, the chemically reacting flow system described herein pertains to a unique reactor design that substantially reduces one or more of the disadvantages of existing systems and methods for non-adiabatic catalytic reactors limited or controlled by heat transfer. Those disadvantages include poor heat transfer [47, 48], high reactor cross-section, low conversion [49, 50], high pressure drop, high reactor volume, channeling, crushing, and high capital costs of multiple alternating heat exchangers and catalytic reactors. The chemically reacting flow system described herein provides a lower pressure drop solution than previously known for non-adiabatic catalytic reactors, particularly those controlled by heat transfer.

3.3. Total enthalpy

The effect of washcoat thickness on the total enthalpy of the exothermic catalytic combustion process is illustrated in Fig. 6 for the reactor system. The washcoat thickness varies from 0.04 to 0.20 mm. The velocity of the endothermic process stream and the exothermic process stream is 2.0 and 0.6 m/s, respectively, at the reactor inlets. For the chemically reacting flow system, the total enthalpy decreases with increasing the thickness of the catalyst washcoats. Preferably, all channels are of the same cross-section and length [51, 52], and adjacent channels are separated by solid walls. Along the flow direction, there is a great change in the total enthalpy of the exothermic catalytic combustion process, as illustrated in Fig. 6. In addition, the wall of the packing is composed of a substrate coated with a catalyst. Consequently, the substrate is preferably metal, and most preferably stainless-steel sheet or foil, such as Aluchrome™ or

Fecralloy™. The substrate may alternatively be a refractory material [53, 54]. The coating may be an alumina-based support containing nickel, a platinum group metal, or other suitable material as the active catalyst. The reactor system may have a significantly improved gas-solid heat transfer, as it may enhance heat transfer through the surfaces of the walls, as illustrated in Fig. 6. The gas to solid heat transfer may increase as compared to a reactor without dividing walls. Even without any additional gas feed, higher volumetric heat transfer coefficients can be achieved with dividing walls as compared to other reactor configurations, as illustrated in Fig. 6. At the surfaces of the walls, the flow may be relatively strong. This flow at or near the surfaces of the walls may therefore cause or increase gas-solid heat transfer between the gas and the dividing walls.

3.4. Effectiveness factors

The effect of washcoat thickness on the effectiveness factor of the endothermic steam reformation reaction is illustrated in Fig. 7 for the reactor system. The washcoat thickness varies from 0.04 to 0.20 mm. The velocity of the endothermic process stream and the exothermic process stream is 2.0 and 0.6 m/s, respectively, at the reactor inlets. For the chemically reacting flow system, the effectiveness factor of the endothermic steam reformation reaction decreases with increasing the thickness of the catalyst washcoats. The effectiveness factor of the endothermic steam reformation reaction is much less than unity, as illustrated in Fig. 7. This is because the temperature of the walls which contains the catalysts will be at temperatures significantly lower than the adiabatic combustion temperature of methanol. These temperatures will depend on a variety of factors [55, 56], including the pressure of the system, the caloric content of the fuel, the partial pressure of oxygen, and the like [57, 58]. Nevertheless, the catalyst will combust the fuel, but it will limit the ultimate temperature to a value lower than the adiabatic combustion temperature because a large fraction of the heat released by the combustion reaction will be absorbed by the endothermic steam reforming reaction on the other side of the dividing walls. The ability to limit combustion temperatures by transferring the heat of combustion from the combustion catalyst to the reforming catalyst through the dividing walls allows the design of smaller reactors operating at lower temperatures. Under this context, the effectiveness factor of the endothermic steam reformation reaction is much less than unity and decreases with increasing the thickness of the catalyst washcoats, as illustrated in Fig. 7. The reforming fuel is mixed with steam to produce a mixture, and the mixture may be at atmospheric pressure or it may be compressed. In the present study, the exothermic and endothermic processes are conducted at a pressure of 0.8 MPa. Therefore, smaller effectiveness factors are obtained for the endothermic steam reformation reaction, as illustrated in Fig. 7 for the reactor system. Nevertheless, reforming catalyst temperatures will be essentially the same as the combustion catalyst temperature, because heat transfer resistances in the dividing walls are typically negligible. The higher diffusion rate of hydrogen is primarily due to hydrogen's lower molecular weight compared to other gaseous species in the reactor system. The diffusion rate is proportional to the square root of the molecular weight of each gas. By removing hydrogen from the reaction region faster than other gaseous species, the equilibrium of the steam reforming and water-gas shift reactions may be shifted, driving the reactions nearer to completion. The intrinsically high surface area of the substrate improves the contact between the feedstock and the catalyst, thereby improving the yield of hydrogen gas in the product stream. A microchannel steam

reforming reactor system in accordance with the present design may be scalable in order to produce hydrogen at a desired rate. For example, multiple microchannel steam reforming reactor systems may be fabricated as interconnectable modules. Furthermore, modules may be added or removed from the stack as needed to increase or decrease the hydrogen production rate. Endothermic catalytic reactions for generating hydrogen with the present design typically require microfabricated components that can perform under harsh operating conditions such as high temperatures, high temperature transients, or corrosive or erosive environments. Such materials should have excellent thermal shock resistance and thermal cycling properties. Further needed are materials that enable features to be fabricated in net-shape and net-size with very high precision.

The contour lines depicted as continuous and smooth lines joining points of equal elevation for temperature, species mole fractions, sensible enthalpy, and total enthalpy are presented in Fig. 8 for the reactor system. The spacing shall be defined as required to provide a useful visualization of performance features through the use of contour lines. The microchannel steam reforming reactor system is designed such that the steam reforming and water-gas shift reactions take place isothermally, as illustrated in Fig. 8. Because the microchannel steam reforming reactor system is very small, with dimensions on the order of several sub-millimeters, the small size can impose substantially isothermal conditions. In general, a higher temperature favors the forward reaction in the case of steam reforming reaction and the reverse reaction in the case of water-gas shift reaction. This is one reason why these two reactions are generally not combined in a single reactor system. However, a microchannel steam reforming reactor system in accordance with the present design may combine both of these reactions in a single device. Both of these reactions may be driven to near completion by continuously removing hydrogen gas from the reaction region. The hydrogen concentration may be increased even further if carbon dioxide is removed from the product stream through a process such as compression and liquefaction. The reactor system described herein can be used as part of a fuel processor to convert methanol to hydrogen for use in a fuel cell which catalytically converts hydrogen and oxygen to water, generating electricity and heat in the process. In a typical fuel cell, hydrogen is fed through a catalyst-containing anode, which converts it to hydrogen ion and electrons. The electrons are diverted to an external circuit to provide electrical energy for an external device such as a motor, then are returned to the cathode side of the fuel cell. Oxygen is fed through the catalyst-containing cathode, where it is catalytically combined with hydrogen ion and electrons to form water. The conversion of methanol is almost complete in the microchannel steam reforming reactor system, as illustrated in Fig. 8. The exothermic combustion of methanol will supply heat to the endothermic steam reforming of methanol to form a hydrogen, carbon monoxide, and carbon dioxide containing mixture. This mixture can be subsequently sent through other reaction steps such as water gas shift and carbon oxide preferential oxidation to produce a hydrogen containing mixture for use in a fuel cell to generate electrical power. The combined system would allow the rapid and cost-effective generation of electrical power from methanol, as illustrated in Fig. 8. The use of the thermal integration design allows the reactor system to be compact, lightweight and cost effective. One advantage of the reactor system is that the dividing wall with the catalyst coating has a small heat capacity and can be heated quickly. Specifically, it can be heated rapidly by preheating the gas flowing through the reaction channels, as illustrated in Fig. 8. This provides a means for rapid start up. For example, a small heater can be provided upstream of the reactor system to heat the

gas mixture entering either the combustion reaction channel or the reforming reaction channel, or both channels. The hot catalyst-coated wall would then have sufficient catalytic activity to combust the fuel components in the combustion reaction channel. The combustion reaction releases heat, further heating the reaction mixture, which in turn transfers heat to the reforming mixture through the heat conductive wall, as illustrated in Fig. 8. This would serve to provide sufficient heat to start the microchannel steam reforming reactor system. The start-up heater could be very small since it would only have to heat the gas mixture to a temperature at which the catalyst would have a high activity. In addition, the hot gas would only have to raise the temperature of the heat conductive wall which has a very low heat capacity and would heat up quickly. The start-up heater may be powered by any suitable means. Typically, a small electric heater is used. In addition, the energy may be supplied by a small battery. On the other hand, methanol is used in the present study as the feedstock fuel. However, other feedstock fuels such as methane, propane, diesel, or the like, may be used in place of methanol. Where the feedstock fuel is a liquid, some pre-heating may be performed to vaporize the liquids prior to input to the microchannel steam reforming reactor system.

4. Conclusions

The present study was focused primarily on the heat and mass transport characteristics of microchannel steam reforming reactor systems for hydrogen production. Computational fluid dynamics simulations were performed to investigate the effects of various key parameters on processes such as chemical reactions or heat and mass transfer in the system. The results indicated that high reforming efficiencies and the desired thermal efficiencies can be achieved. Methanol breakthrough is negligible, but the reactor system must be operated using a stoichiometric or lean fuel-air mixture. The chemically reacting flow system pertains to a unique reactor design that substantially reduces one or more of the disadvantages of existing systems and methods for non-adiabatic catalytic reactors limited or controlled by heat transfer. The effectiveness factor of the endothermic steam reformation reaction is much less than unity. The sensible and effectiveness factor depend heavily upon the thickness of the catalyst washcoats. As the washcoat thickness increases, the sensible enthalpy increases but the total enthalpy and effectiveness factor decrease. The use of the thermal integration design allows the reactor system to be compact, lightweight and cost effective.

Declarations

Declaration of competing interest

The authors declare that there is no conflict of interest.

References

1. A. Faridkhou, J.-N. Tourvieille, and F. Larachi. Reactions, hydrodynamics and mass transfer in micro-packed beds-Overview and new mass transfer data. Chemical Engineering and Processing: Process Intensification, Volume 110, 2016, Pages 80–96.

2. M.W. Losey, M.A. Schmidt, and K.F. Jensen. Microfabricated multiphase packed-bed reactors: Characterization of mass transfer and reactions. Industrial & Engineering Chemistry Research, Volume 40, Issue 12, 2001, Pages 2555–2562.
3. L.H. Macfarlan, M.T. Phan, and R.B. Eldridge. Methodologies for predicting the mass transfer performance of structured packings with computational fluid dynamics: A review. *Chemical Engineering and Processing - Process Intensification*, Volume 172, 2022, Article Number 108798.
4. S.A. Owens, M.R. Perkins, R.B. Eldridge, K.W. Schulz, and R.A. Ketcham. Computational fluid dynamics simulation of structured packing. Industrial & Engineering Chemistry Research, Volume 52, Issue 5, 2013, Pages 2032–2045.
5. F. Kapteijn and J.A. Moulijn. Structured catalysts and reactors - Perspectives for demanding applications. Catalysis Today, Volume 383, 2022, Pages 5–14.
6. K. Pangarkar, T.J. Schildhauer, J.R.V. Ommen, J. Nijenhuis, F. Kapteijn, and J.A. Moulijn. Structured packings for multiphase catalytic reactors. Industrial & Engineering Chemistry Research, Volume 47, Issue 10, 2008, Pages 3720–3751.
7. E. Tronconi, G. Groppi, and C.G. Visconti. Structured catalysts for non-adiabatic applications. Current Opinion in Chemical Engineering, Volume 5, 2014, Pages 55–67.
8. R.E. Hayes, A. Rojas, and J. Mmbaga. The effective thermal conductivity of monolith honeycomb structures. Catalysis Today, Volume 147, Supplement, 2009, Pages S113-S119.
9. I. Cornejo, P. Nikrityuk, and R.E. Hayes. Heat and mass transfer inside of a monolith honeycomb: From channel to full size reactor scale. Catalysis Today, Volume 383, 2022, Pages 110–122.
10. C.G. Visconti, G. Groppi, and E. Tronconi. Accurate prediction of the effective radial conductivity of highly conductive honeycomb monoliths with square channels. Chemical Engineering Journal, Volume 223, 2013, Pages 224–230.
11. E.M. Moghaddam, E.A. Foumeny, A.I. Stankiewicz, and J.T. Padding. Heat transfer from wall to dense packing structures of spheres, cylinders and Raschig rings. Chemical Engineering Journal, Volume 407, 2021, Article Number 127994.
12. H. Sadeghifar and A.A.S. Kordi. A new and applicable method to calculate mass and heat transfer coefficients and efficiency of industrial distillation columns containing structured packings. Energy, Volume 36, Issue 3, 2011, Pages 1415–1423.
13. R.C. Ramaswamy, P.A. Ramachandran, and M.P. Duduković. Coupling exothermic and endothermic reactions in adiabatic reactors. Chemical Engineering Science, Volume 63, Issue 6, 2008, Pages 1654–1667.
14. M.R. Rahimpour, M.R. Dehnavi, F. Allahgholipour, D. Iranshahi, and S.M. Jokar. Assessment and comparison of different catalytic coupling exothermic and endothermic reactions: A review. Applied Energy, Volume 99, 2012, Pages 496–512.
15. M. Mbodji, J.-M. Commenge, and L. Falk. Preliminary design and simulation of a microstructured reactor for production of synthesis gas by steam methane reforming. Chemical Engineering Research and Design, Volume 92, Issue 9, 2014, Pages 1728–1739.

16. G. Bozzano and F. Manenti. Efficient methanol synthesis: Perspectives, technologies and optimization strategies. Progress in Energy and Combustion Science, Volume 56, 2016, Pages 71–105.
17. A. Daisley, J.S.J. Hargreaves, R. Hermann, Y. Poya, and Y. Wang. A comparison of the activities of various supported catalysts for ammonia synthesis. Catalysis Today, Volume 357, 2020, Pages 534–540.
18. E. Baraj, K. Ciahotný, and T. Hlinčík. The water gas shift reaction: Catalysts and reaction mechanism. Fuel, Volume 288, 2021, Article Number 119817.
19. R.C. Brown. Process intensification through directly coupled autothermal operation of chemical reactors. Joule, Volume 4, Issue 11, 2020, Pages 2268–2289.
20. G. Zhang, W. Jin, N. Xu. Design and fabrication of ceramic catalytic membrane reactors for green chemical engineering applications. Engineering, Volume 4, Issue 6, 2018, Pages 848–860.
21. S. Afandizadeh and E.A. Foumeny. Design of packed bed reactors: guides to catalyst shape, size, and loading selection. Applied Thermal Engineering, Volume 21, Issue 6, 2001, Pages 669–682.
22. Y. Ding, Y. He, N.T. Cong, W. Yang, and H. Chen. Hydrodynamics and heat transfer of gas-solid two-phase mixtures flowing through packed beds - a review. Progress in Natural Science, Volume 18, Issue 10, 2008, Pages 1185–1196.
23. Z. Xie, S. Wang, and Y. Shen. CFD-DEM modelling of the migration of fines in suspension flow through a solid packed bed. Chemical Engineering Science, Volume 231, 2021, Article Number 116261.
24. E. Achenbach. Heat and flow characteristics of packed beds. Experimental Thermal and Fluid Science, Volume 10, Issue 1, 1995, Pages 17–27.
25. C.F. Petre, F. Larachi, I. Iliuta, and B.P.A. Grandjean. Pressure drop through structured packings: Breakdown into the contributing mechanisms by CFD modeling. Chemical Engineering Science, Volume 58, Issue 1, 2003, Pages 163–177.
26. P. Valluri, O.K. Matar, G.F. Hewitt, and M.A. Mendes. Thin film flow over structured packings at moderate Reynolds numbers. Chemical Engineering Science, Volume 60, Issue 7, 2005, Pages 1965–1975.
27. L.H. Macfarlan, A.F. Seibert, M.T. Phan, and R.B. Eldridge. CFD-based study on structured packing geometry. Chemical Engineering Science, Volume 243, 2021, Article Number 116767.
28. L. Li, W. Xie, Z. Zhang, and S. Zhang. Pressure drop in packed beds with horizontally or vertically stratified structure. Nuclear Engineering and Technology, Volume 52, Issue 11, 2020, Pages 2491–2498.
29. L. Spiegel, P. Bomio, and R. Hunkeler. Direct heat and mass transfer in structured packings. Chemical Engineering and Processing: Process Intensification, Volume 35, Issue 6, 1996, Pages 479–485.
30. K. Pangarkar, T.J. Schildhauer, J.R.V. Ommen, J. Nijenhuis, J.A. Moulijn, and F. Kapteijn. Heat transport in structured packings with co-current downflow of gas and liquid. Chemical Engineering Science, Volume 65, Issue 1, 2010, Pages 420–426.
31. P. Qian, J. Wang, Z. Wu, J. Yang, and Q. Wang. Performance comparison of methane steam reforming in a randomly packed bed and a grille-sphere composite packed bed. Energy Conversion and Management, Volume 193, 2019, Pages 39–51.

32. A.T. Naseri, B.A. Peppley, and J.G. Pharoah. A systematic parametric study on the effect of a catalyst coating microstructure on its performance in methane steam reforming. International Journal of Hydrogen Energy, Volume 40, Issue 46, 2015, Pages 16086–16095.
33. T.J. Schildhauer, K. Pangarkar, J.R.V. Ommen, J. Nijenhuis, J.A. Moulijn, and F. Kapteijn. Heat transport in structured packings with two-phase co-current downflow. *Chemical Engineering Journal*, Volumes 185–186, 2012, Pages 250–266.
34. E.M. Moghaddam, E.A. Foumeny, A.I. Stankiewicz, and J.T. Padding. Multiscale modelling of wall-to-bed heat transfer in fixed beds with non-spherical pellets: From particle-resolved CFD to pseudo-homogenous models. Chemical Engineering Science, Volume 236, 2021, Article Number 116532.
35. J.J. Lerou, A.L. Tonkovich, L. Silva, S. Perry, and J. McDaniel. Microchannel reactor architecture enables greener processes. Chemical Engineering Science, Volume 65, Issue 1, 2010, Pages 380–385.
36. A. Tonkovich, D. Kuhlmann, A. Rogers, J. McDaniel, S. Fitzgerald, R. Arora, and T. Yuschak. Microchannel technology scale-up to commercial capacity. Chemical Engineering Research and Design, Volume 83, Issue 6, 2005, Pages 634–639.
37. A.Y. Tonkovich, S. Perry, Y. Wang, D. Qiu, T. LaPlante, and W.A. Rogers. Microchannel process technology for compact methane steam reforming. *Chemical Engineering Science*, Volume 59, Issues 22–23, 2004, Pages 4819–4824.
38. A.L.Y. Tonkovich, B. Yang, S.T. Perry, S.P. Fitzgerald, and Y. Wang. From seconds to milliseconds to microseconds through tailored microchannel reactor design of a steam methane reformer. Catalysis Today, Volume 120, Issue 1, 2007, Pages 21–29.
39. Y. Chen, C. Zhang, R. Wu, and M. Shi. Methanol steam reforming in microreactor with constructal tree-shaped network. Journal of Power Sources, Volume 196, Issue 15, 2011, Pages 6366–6373.
40. J.-S. Suh, M.-T. Lee, R. Greif, And C.P. Grigoropoulos. A study of steam methanol reforming in a microreactor. Journal of Power Sources, Volume 173, Issue 1, 2007, Pages 458–466.
41. W. Wiese, B. Emonts, and R. Peters. Methanol steam reforming in a fuel cell drive system. Journal of Power Sources, Volume 84, Issue 2, 1999, Pages 187–193.
42. D. Ipsakis, M. Ouzounidou, S. Papadopoulou, P. Seferlis, and S. Voutetakis. Dynamic modeling and control analysis of a methanol autothermal reforming and PEM fuel cell power system. Applied Energy, Volume 208, 2017, Pages 703–718.
43. T.L. Reitz, S. Ahmed, M. Krumpelt, R. Kumar, and H.H. Kung. Characterization of CuO/ZnO under oxidizing conditions for the oxidative methanol reforming reaction. *Journal of Molecular Catalysis A: Chemical*, Volume 162, Issues 1–2, 2000, Pages 275–285.
44. B.A. Peppley, J.C. Amphlett, L.M. Kearns, and R.F. Mann. Methanol-steam reforming on $Cu/ZnO/Al_2O_3$ catalysts. Part 2. A comprehensive kinetic model. *Applied Catalysis A: General*, Volume 179, Issues 1–2, 1999, Pages 31–49.
45. G.-G. Park, D.J. Seo, S.-H. Park, Y.-G. Yoon, C.-S. Kim, and W.-L. Yoon. Development of microchannel methanol steam reformer. *Chemical Engineering Journal*, Volume 101, Issues 1–3, 2004, Pages 87–92.

46. G.-G. Park, S.-D. Yim, Y.-G. Yoon, W.-Y. Lee, C.-S. Kim, D.-J. Seo, and K. Eguchi. Hydrogen production with integrated microchannel fuel processor for portable fuel cell systems. Journal of Power Sources, Volume 145, Issue 2, 2005, Pages 702–706.
47. R.C. Brown. Process intensification through directly coupled autothermal operation of chemical reactors. Joule, Volume 4, Issue 11, 2020, Pages 2268–2289.
48. L.J.J. Catalan and E. Rezaei. Modelling the hydrodynamics and kinetics of methane decomposition in catalytic liquid metal bubble reactors for hydrogen production. International Journal of Hydrogen Energy, Volume 47, Issue 12, 2022, Pages 7547–7568.
49. E.A. Daymo, M. Hettel, O. Deutschmann, and G.D. Wehinger. Accelerating particle-resolved CFD simulations of catalytic fixed-bed reactors with DUO. Chemical Engineering Science, Volume 250, 2022, Article Number 117408.
50. M. Shah, D. West, and V. Balakotaiah. Analysis of temperature patterns in shallow-bed autothermal catalytic reactors. *Chemical Engineering Journal*, Volume 437, Part 2, 2022, Article Number 135027.
51. S. Bai, W.-S. Li, W. Liu, Y. Luo, G.-W. Chu, and J.-F. Chen. Micromixing efficiency intensification of a millimeter channel reactor in the high gravity field. Chemical Engineering Science, Volume 251, 2022, Article Number 117407.
52. M.P. Singh, M. Saeed, and A.S. Berrouk. Non linear stability analysis of supercritical water cooled reactor: Parallel channels configuration. Progress in Nuclear Energy, Volume 147, 2022, Article Number 104194.
53. F. Vargas, E. Restrepo, J.E. Rodríguez, F. Vargas, L. Arbeláez, P. Caballero, J. Arias, E. López, G. Latorre, and G. Duarte. Solid-state synthesis of mullite from spent catalysts for manufacturing refractory brick coatings. Ceramics International, Volume 44, Issue 4, 2018, Pages 3556–3562.
54. T.H. Lee, U. Jung, H.B. Im, K.D. Kim, J. Kim, Y.-E. Kim, D. Song, and K.Y. Koo. Comparative evaluation of Ru-coated fecralloy and SiC monolithic catalysts in catalytic partial oxidation of natural gas for hydrogen production. Journal of Industrial and Engineering Chemistry, Volume 110, 2022, Pages 178–187.
55. P.L. Suryawanshi, S.P. Gumfekar, B.A. Bhanvase, S.H. Sonawane, and M.S. Pimplapure. A review on microreactors: Reactor fabrication, design, and cutting-edge applications. Chemical Engineering Science, Volume 189, 2018, Pages 431–448.
56. R. Munirathinam, J. Huskens, and W. Verboom. Supported catalysis in continuous-flow microreactors. Advanced Synthesis and Catalysis, Volume 357, Issue 6, 2015, Pages 1093–1123.
57. Z. Dong, Z. Wen, F. Zhao, S. Kuhn, and T. Noël. Scale-up of micro- and milli-reactors: An overview of strategies, design principles and applications. Chemical Engineering Science: X, Volume 10, 2021, Article Number 100097.
58. I. Rossetti and M. Compagnoni. Chemical reaction engineering, process design and scale-up issues at the frontier of synthesis: Flow chemistry. Chemical Engineering Journal, Volume 296, 2016, Pages 56–70.

Figures

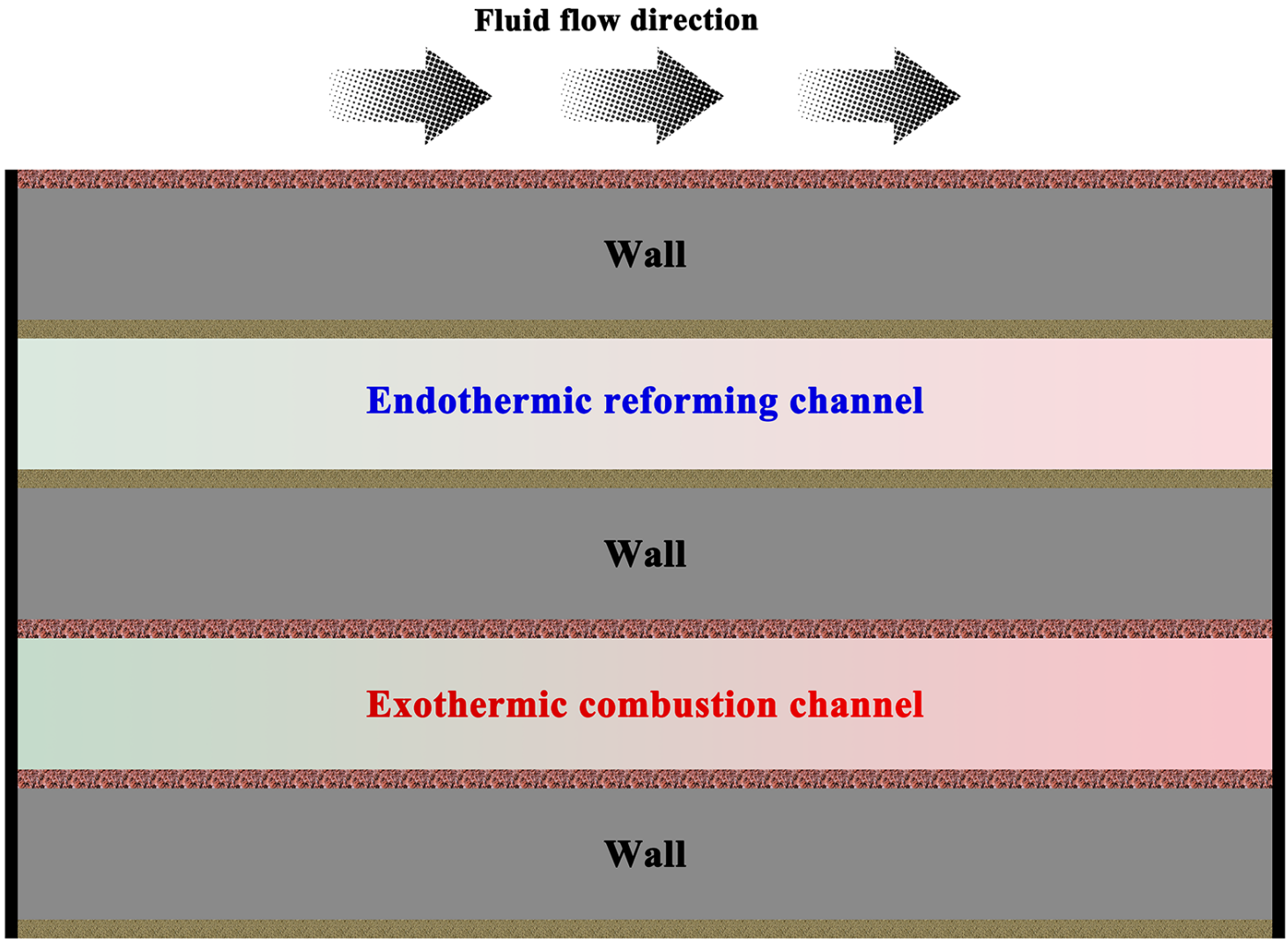

Figure 1

Schematic illustration of the microchannel steam reforming reactor system used for the production of hydrogen by steam reforming of methanol. The walls have a uniform structure throughout their cross-section and along their longitudinal length. The fluid flow direction is indicated by arrows.

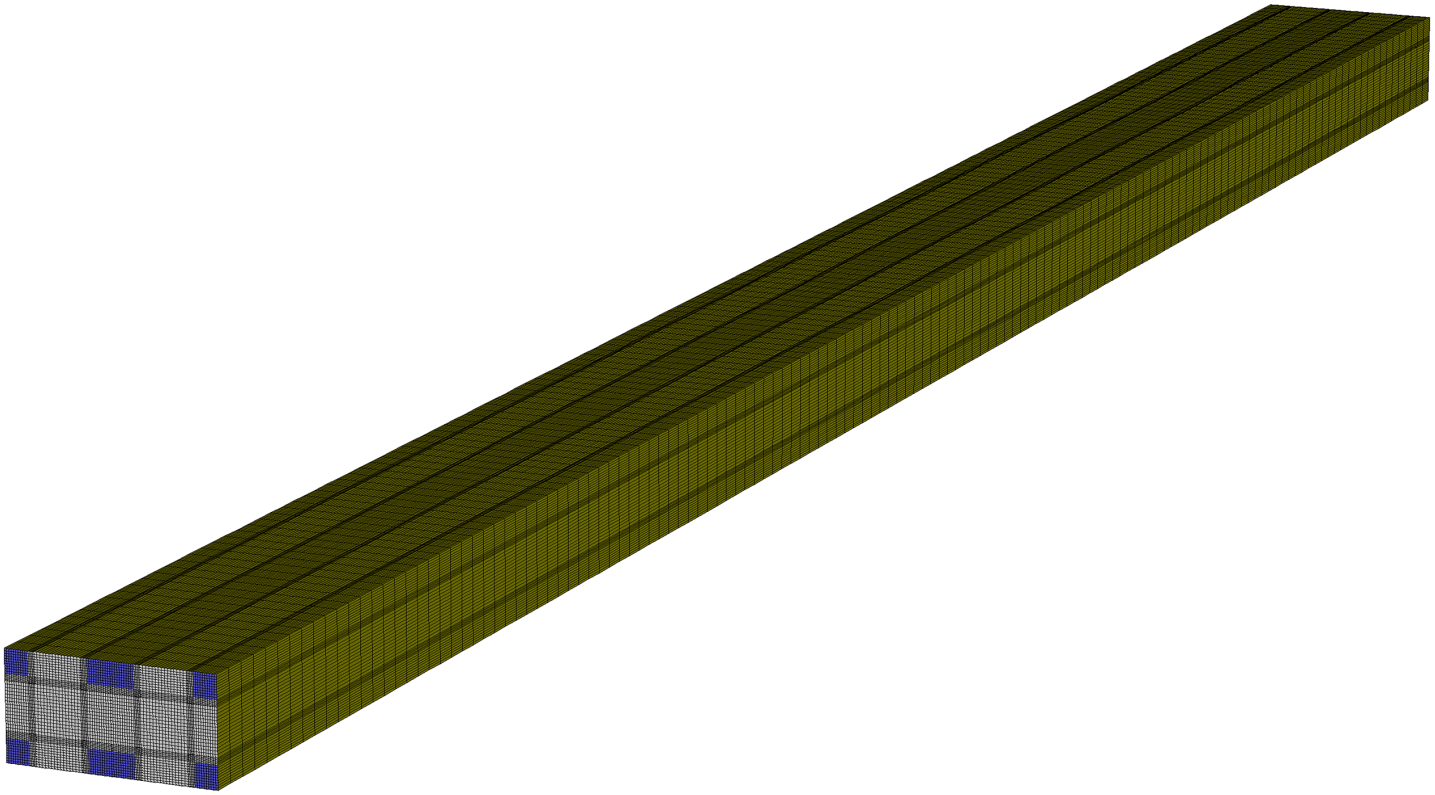

Figure 2

Schematic representation of the typical mesh used for the reactor system. A mesh independence study is carried out and the solution is independent of the mesh resolution.

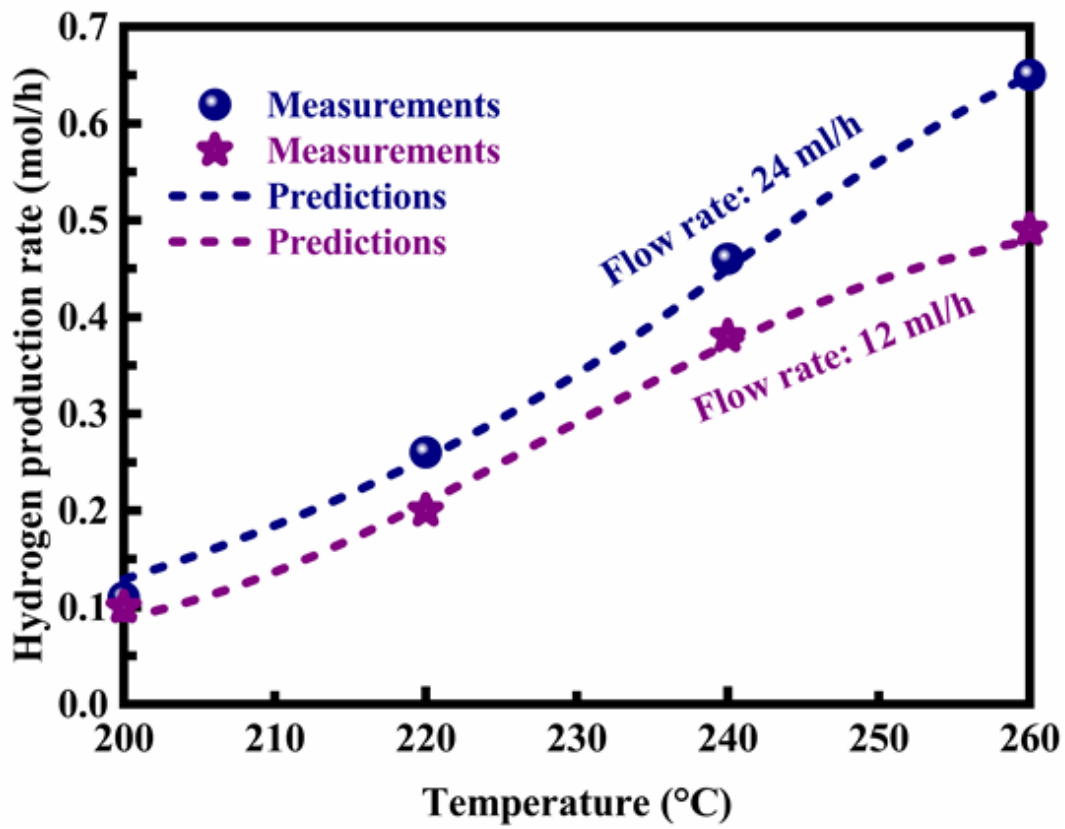

Figure 3

Hydrogen production rate predicted by the model as a function of temperature. The measurement results of the variables of interest are also presented for the purpose of comparison.

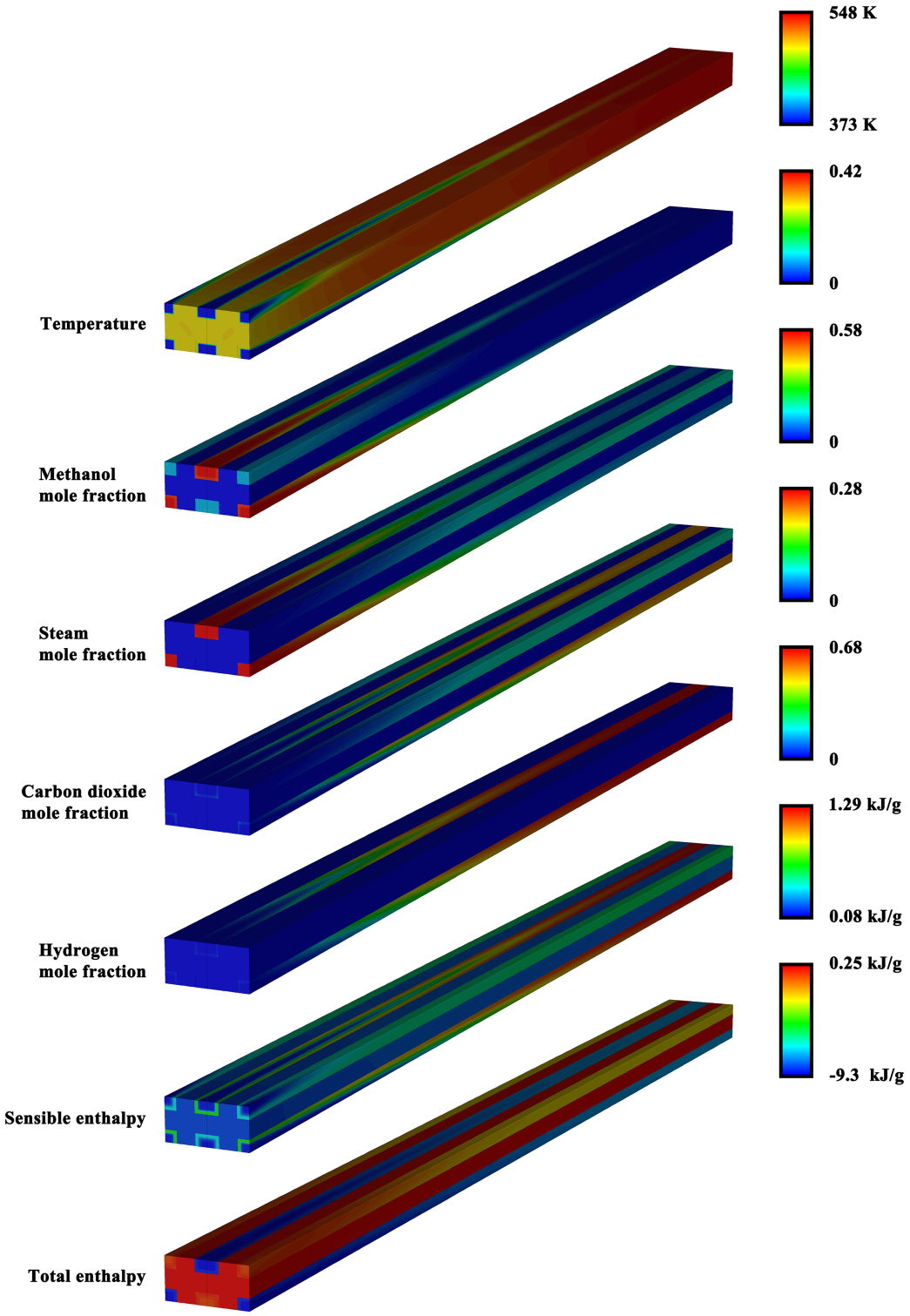

Figure 4

Contour plots of temperature, species mole fractions, sensible enthalpy, and total enthalpy for the reactor system. The effective thermal conductivity of the washcoat is 16 W/(m·K) at room temperature. The porosity of the washcoat is 0.5. The velocity of the endothermic process stream and the exothermic process stream is 2.0 and 0.6 m/s, respectively, at the reactor inlets.

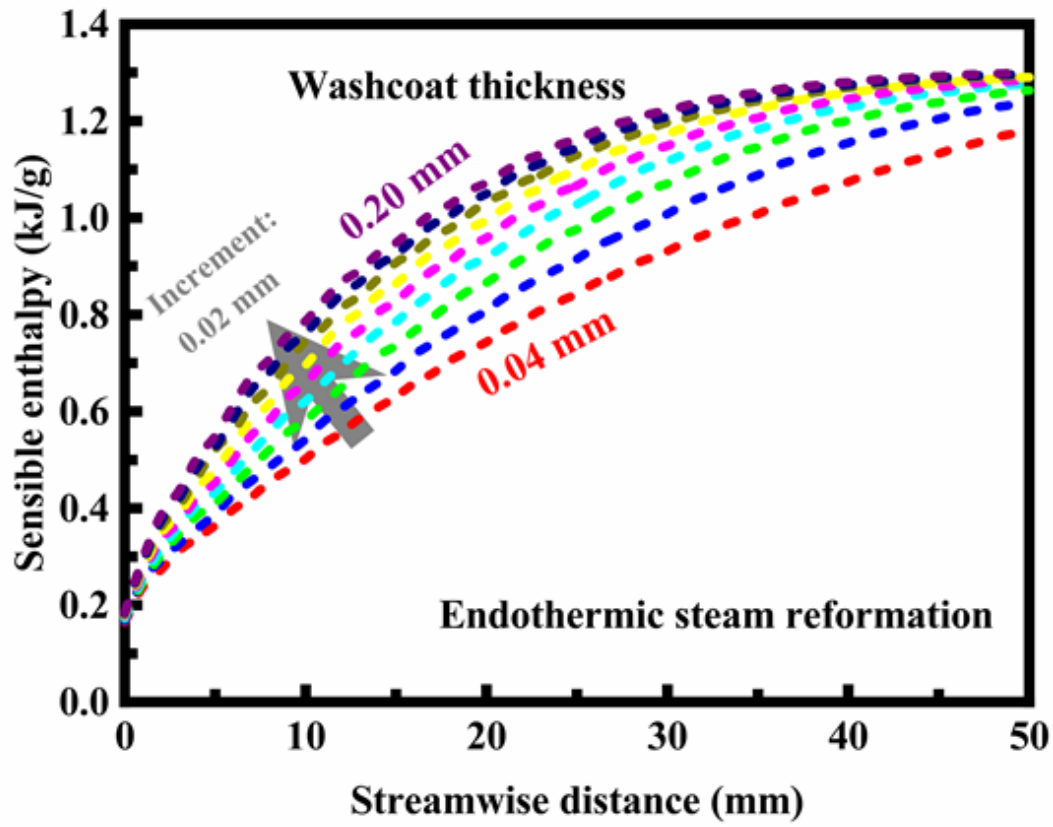

Figure 5

Effect of washcoat thickness on the sensible enthalpy of the endothermic steam reformation process. The washcoat thickness varies from 0.04 to 0.20 mm. The velocity of the endothermic process stream and the exothermic process stream is 2.0 and 0.6 m/s, respectively, at the reactor inlets.

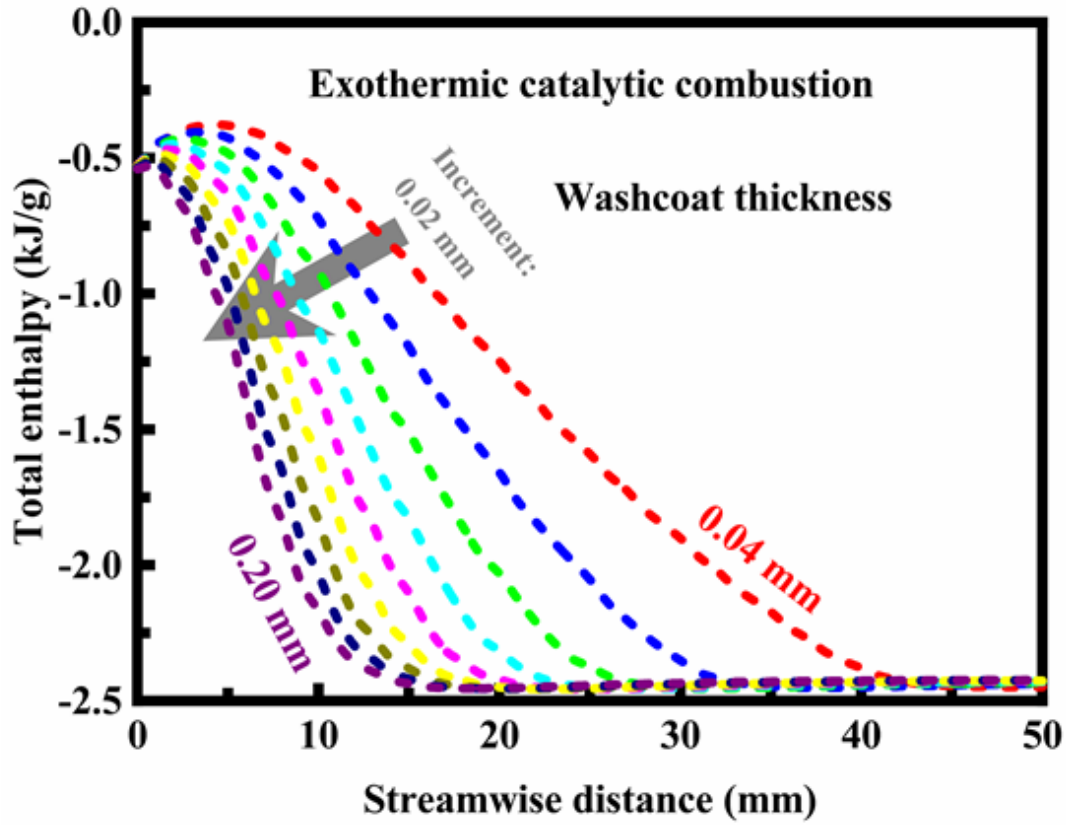

Figure 6

Effect of washcoat thickness on the total enthalpy of the exothermic catalytic combustion process. The washcoat thickness varies from 0.04 to 0.20 mm. The velocity of the endothermic process stream and the exothermic process stream is 2.0 and 0.6 m/s, respectively, at the reactor inlets.

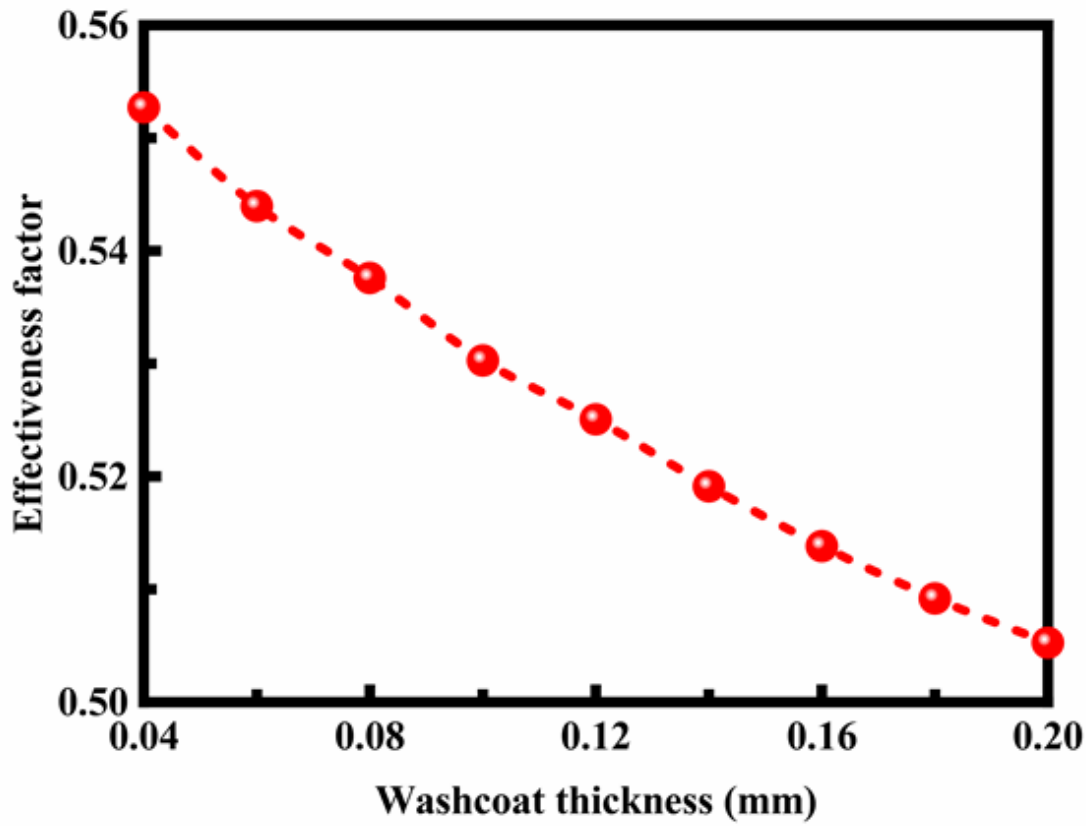

Figure 7

Effect of washcoat thickness on the effectiveness factor of the endothermic steam reformation reaction. The exothermic and endothermic processes are conducted at a pressure of 0.8 MPa. The washcoat thickness varies from 0.04 to 0.20 mm. The velocity of the endothermic process stream and the exothermic process stream is 2.0 and 0.6 m/s, respectively, at the reactor inlets.

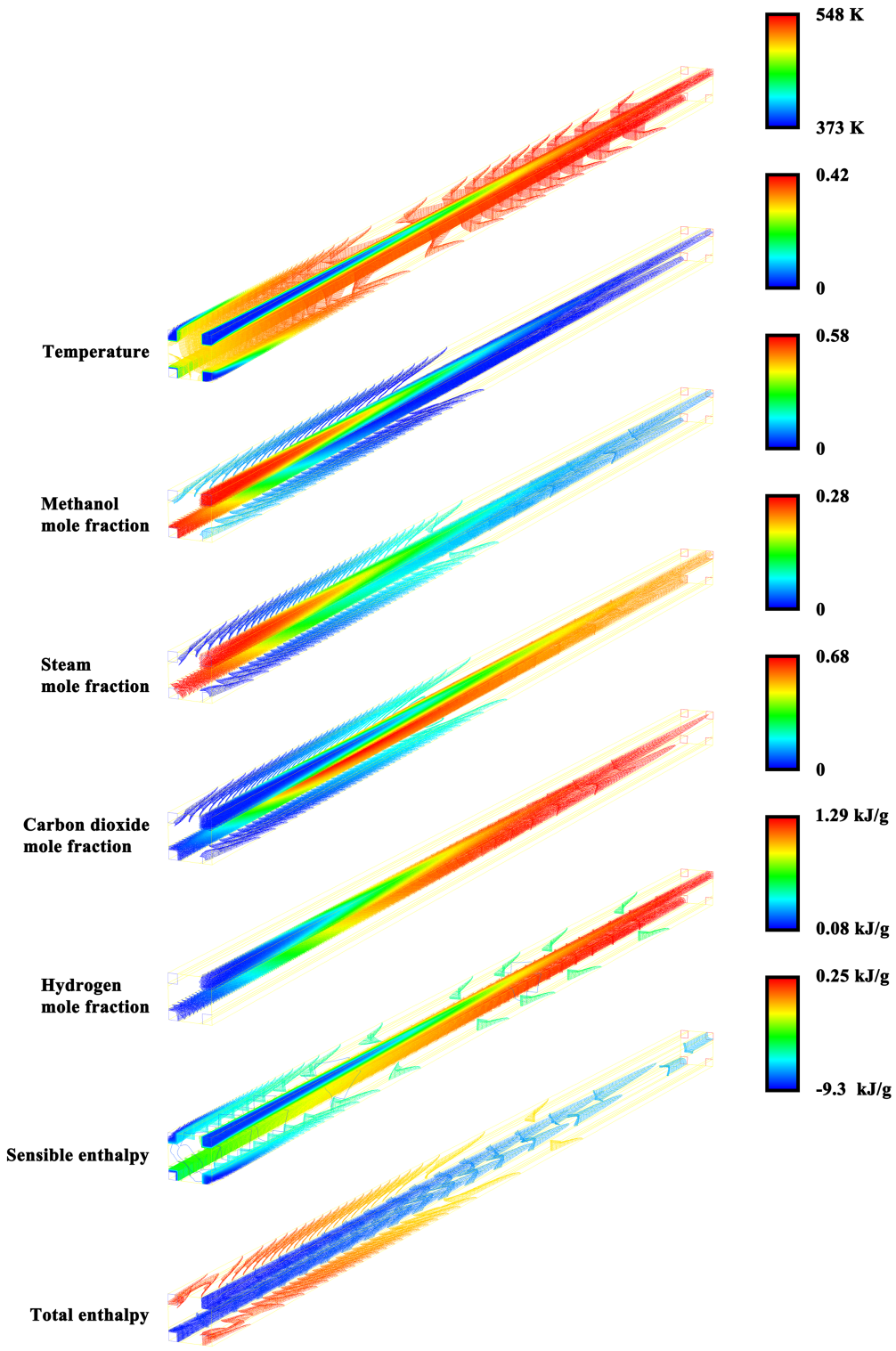

Figure 8

Contour lines depicted as continuous and smooth lines joining points of equal elevation for the temperature, species mole fractions, sensible enthalpy, and total enthalpy of the reactor system. The velocity of the endothermic process stream and the exothermic process stream is 2.0 and 0.6 m/s, respectively, at the reactor inlets.